Contents lists available at ScienceDirect

Transactions of Nonferrous Metals Society of China

36(2026) 766−779

www.tnmsc.cn

Evolution of grain orientation and slip mode in gradient AZ31 magnesium alloy sheets with multiple texture components

Wen-tao NIU [a], Feng LI [a,b,c,*], Jia-yang ZHANG [a,**], Lu SUN [a], Zi-yi WANG [a]

[a] School of Materials Science and Chemical Engineering, Harbin University of Science and Technology, Harbin 150040, China;

[b] Key Laboratory of Advanced Manufacturing and Intelligent Technology, Ministry of Education, Harbin University of Science and Technology, Harbin 150080, China;

[c] Heilongjiang Provincial Key Laboratory of Light Metal Materials Modification & Green Forming Technology, Harbin University of Science and Technology, Harbin 150040, China

Abstract: To investigate the evolution of grain orientation and slip modes in magnesium alloys with multiple texture components, an AZ31 gradient-structured magnesium alloy sheet was fabricated using hard plate rolling (HPR). The changes in texture and slip modes under different reductions were examined. The results demonstrate that the AZ31 magnesium alloy sheets display a self-epitaxial gradient structure, with the best mechanical properties observed at rolling temperature of 673 K and reduction of 50%. Significant changes in texture type and strength are observed along the normal direction (ND) of the sheet. The coarse-grain region exhibits a bimodal texture aligned with the rolling direction. These texture variations enhance the stress distribution at the fine grain−coarse grain interface, influencing the grain orientation and the activation of different slip modes, thus improving the mechanical properties of gradient-structured magnesium alloy sheets. This approach offers a new strategy for the fabrication of high-performance magnesium alloy sheets.

Keywords: hard plate rolling; AZ31 magnesium alloy sheet; gradient structure; texture components; grain orientation

1 Introduction

The growing energy crisis and environmental concerns have increased the demand for lightweight equipment in high-end industries, resulting in a rise in the consumption of high-performance sheet metal [1−3]. As a result, research and development aimed at producing high-quality sheet metal have become essential for enhancing a nation's scientific and technological capabilities and fostering industrial economic growth [4−6]. The rolling process has proven to be the most effective method for producing high-performance deformed magnesium alloy (Mg alloy) sheets, and it remains a central focus of current research [7−9]. Recent studies have shown that combining rolling with heat treatment improves the properties of magnesium alloy sheets. For example, CHANG et al [10] used a combined rolling and heat treatment process to prepare AZ31 magnesium alloy sheets, achieving significant grain refinement and enhanced tensile strength. Additionally, DEL et al [11] applied cumulative rolling to achieve notable grain refinement in AZ61 magnesium alloy sheets, with increased microstructure uniformity as the number of rolling passes increased.

However, during the rolling process, magnesium alloys quickly develop a strong basal

Corresponding author: *Feng LI, Tel: +86-13303668051, E-mail: fli@hrbust.edu.cn;
**Jia-yang ZHANG, Tel: +86-15046116904, E-mail: zjy92316904@163.com

https://doi.org/10.1016/S1003-6326(25)66996-2
Received 31 May 2024; accepted 25 March 2025

texture, and the limited number of sliding systems that can be activated at room temperature restricts their ability to deform, resulting in significant anisotropy [12−14]. SINGH and SCHWARZER [15] explored texture evolution in rolled magnesium alloys and found that the texture composition was strongly influenced by the rolling process. LIANG et al [16] examined the mechanical properties and texture evolution of rolled AZ31 magnesium alloy and reported that the basal texture strength increases with reduction, and the displacement of the grain *c*-axis is associated with the activation of non-basal slip. Therefore, understanding the influence of texture development on slip system activation, strength, and ductility during rolling is crucial for enhancing the formability of magnesium alloy sheets [17−19].

Recently, the incorporation of heterogeneous structures [20], such as gradient structures [21], non-uniform lamellar structures [22], and bimodal structures [23], has been shown to increase the strength and ductility of magnesium alloy sheets [24]. Research has revealed that improvements in mechanical properties are attributed to non-uniform texture components [25]. For example, LIU et al [26] investigated the characteristics of the textural components in heterogeneously structured magnesium alloys. They reported that coarse grain (CG) layers exhibit bimodal textures, whereas fine grain (FG) layers display random textures, leading to interactions between basal and non-basal slip systems that significantly enhance the mechanical properties. DUAN et al [27] prepared a gradient structure of AZ31 magnesium alloy via surface mechanical attrition treatment (SMAT) and reported that FG layers exhibit more random grain orientations, weakened texture strength, and reduced anisotropy in mechanical properties. AMIRI and FERESHTEH-SANIEE [28] prepared a Mg−13Gd alloy with a non-uniform lamellar structure through extrusion, revealing significant differences in texture components between the FG and CG regions, with plasticity improvements primarily due to weakened fine grain structures.

A new technique, hard plate rolling (HPR), has been introduced, facilitating controlled micro-structural changes in the thickness direction by adding a hard plate to the outer surface of the rolled sheet [29]. WANG et al [30] utilized HPR to fabricate AZ91 magnesium alloy sheets, achieving significant improvements in both strength and ductility without the occurrence of edge cracks, even under substantial reductions. LI et al [31] explored the microstructure evolution and tensile properties of AZ91 magnesium alloy sheets processed via HPR, attributing the enhanced strength to the weakening of basal textures and the strengthening of grain boundaries in the FG regions. Earlier research demonstrated the successful creation of AZ31 magnesium alloy sheets with gradient structures, exhibiting non-uniform grain sizes and texture component distributions along the normal direction (ND) via HPR [32]. However, most previous studies have concentrated on grain boundary strengthening and texture weakening, overlooking the sliding mechanisms and mechanical behavior of various texture components in magnesium sheets, particularly those with gradient structures. This study seeks to address this gap in understanding.

2 Experimental

2.1 Process principle

The principle of the AZ31 gradient structure of a magnesium alloy sheet via HPR is illustrated in Fig. 1. When the individual magnesium plate was subjected to the action of the hard plate, it simultaneously formed a soft plate together with another magnesium plate. During the rolling process, the side near the hard plate underwent significant deformation, leading to an uneven distribution of deformation along the ND of the magnesium alloy slab, as corroborated by recent research findings [33]. The recrystallization driving force was more pronounced near the surface adjacent to the hard plate, where grains were fully refined under the combined effects of external stress and dynamic recrystallization. Conversely, in the center of the sheet, deformation was minimal, the recrystallization driving force was inadequate, and grain refinement was less pronounced. This region contained large deformed grains, resulting in a gradient structure within the magnesium alloy sheet, transitioning from fine grains to coarse grains along the ND.

2.2 Research program

AZ31 magnesium alloy was cut into slabs measuring 60 mm × 30 mm × 4 mm, then homogenized in a box resistance furnace at 693 K for 12 h, and air-cooled to room temperature. During the rolling process, a 304 stainless steel hard plate was

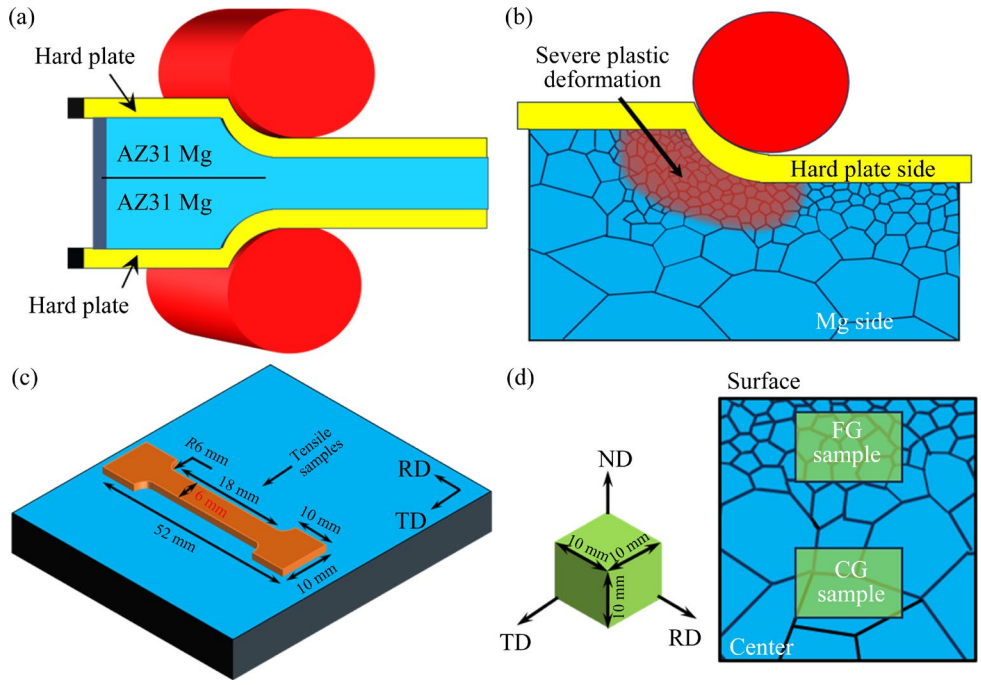

Fig. 1 Principle of HPR AZ31 magnesium alloy sheet with gradient structure: (a) Schematic diagram of process; (b) Schematic diagram of gradient structure formation; (c) Schematic diagram of tensile specimen size and sampling location; (d) Sampling size and sampling position diagram of EBSD sample

attached to the outer surfaces of two magnesium alloy sheets. Prior to rolling, the sheet surfaces were polished with #80 sandpaper, followed by cleaning with acetone solution to remove surface oil and impurities. The samples were then rinsed with alcohol and air-dried. After stacking the two sheets, they were secured to the hard plate using an iron wire (d=0.2 mm). To prevent the magnesium alloy from adhering to the stainless steel during rolling, a layer of high-temperature boron nitride insulating agent was applied to the contact surfaces. The samples were heated to 673 K in a box-shaped resistance oven and maintained at this temperature for 10 min. The experimental setup consisted of a two-roll mill (d200 mm × 250 mm) operating at a speed of 16 rad/s. The heated slabs were fed into the mill for rolling, with reductions of 40%, 50%, and 60% to produce gradient magnesium alloy sheet samples with different specifications. For convenience, these samples are referred to as 40%-sheets, 50%-sheets, and 60%-sheets. The rolling direction is defined as RD, and the normal direction of the plate is designated as ND.

2.3 Mechanical property characterization

The mechanical properties of the rolled magnesium alloy sheet were tested. The sample was cut into the shape of a dog bone using the electric sparkline, as shown in Fig. 1(c). After being cut, the surface of the sample was polished to remove acceptable defects. The uniaxial sample strain along the RD was measured via a CMT5105 electronic universal testing machine at room temperature at a strain rate of 1.0×10^{-3} s^{-1}. The samples were tested three times under each condition and averaged to ensure the accuracy of the results. Professional data processing software was used to process and analyze the data results, and the stress–strain curve was adjusted to obtain the actual strain–real hardening rate curve, which was used to characterize the work hardening ability of the sample [34].

2.4 Microscopic characterization

The microstructural difference play a significant role in determining the mechanical properties and formability of a material. The EBSD sample was taken from the ND of the sheet, with its size and position shown in Fig. 1(d). The observation surface was polished using 80#, 200#, 1000#, 3000#, and 5000# grit sandpapers. Afterward, the EBSD sample was prepared through electrolytic polishing. A mixture of phosphoric acid and alcohol (in a

volume ratio of 3:5) was selected as the polishing solution, and the polishing process was carried out for 3 and 5 min at currents of 0.3 and 0.2 A, respectively. The EBSD test was performed using a Quanta 200F field emission scanning electron microscope. The test stand was tilted at 70°, with a step size of 1 μm. The collected data were analyzed using Channel 5 software.

3 Results

3.1 Mechanical properties

Owing to the changes in the stress state and deformation conditions, the structural shape and development characteristics of the gradient structure inevitably affect the mechanical properties of the sheet and determine its quality after rolling. Figure 2 shows the engineering stress–strain and true strain–strain hardening rate curves of the AZ31 magnesium alloy rolled by HPR during RD uniaxial tensile testing under different conditions. As shown in the figure, the yield strength (YS) and ultimate tensile strength (UTS) of the 50%-sheets were 168.2 and 268.3 MPa, respectively, and the elongation (EL) of the 50%-sheets reached 28.3%, indicating a better combination of strength and ductility. The elongation was significantly greater than that of the 40%-sheet and 60%-sheet samples (22.6% and 19.9%, respectively).

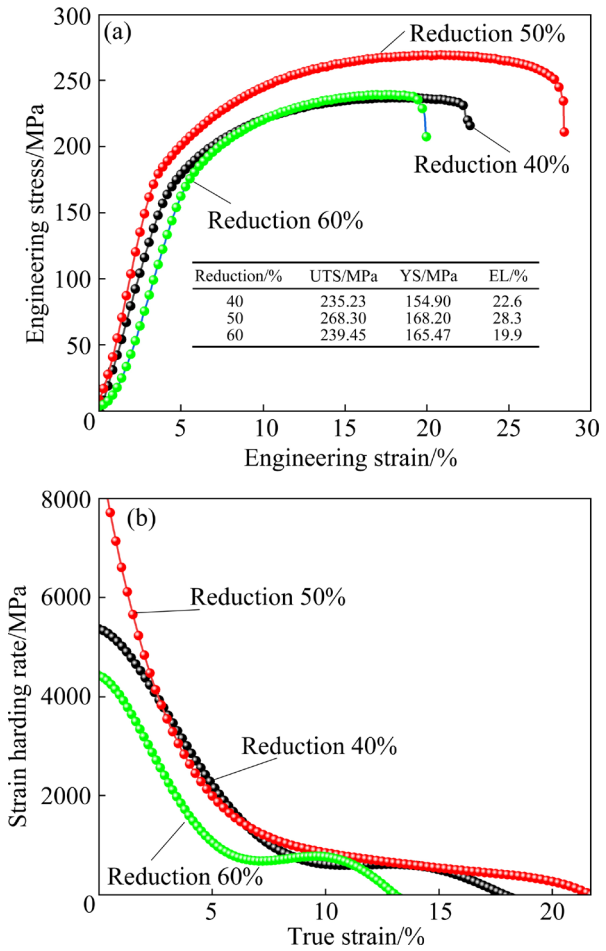

Reduction/%	UTS/MPa	YS/MPa	EL/%
40	235.23	154.90	22.6
50	268.30	168.20	28.3
60	239.45	165.47	19.9

Fig. 2 Engineering stress–strain curves (a) and true strain–strain hardening rate curves (b) of samples under different conditions

The work hardening rate is the main factor affecting the tensile strength and uniform elongation of materials. Figure 2(b) shows the strain hardening rate curve, which was calculated from the stress–strain curve (Fig. 2(a)). The expression of the strain hardening rate is $\theta=\mathrm{d}\sigma/\mathrm{d}\varepsilon$, where σ is the true stress and ε is the true strain. The work hardening capacity of 50% of the sheets was greater than that of the other two states. With the gradual increase in true strain, the work hardening rates of all samples gradually decrease. At this time, the work hardening rate curve of 50%-sheets decreases steadily without any obvious turning point, and the fluctuation is small, so a relatively stable work hardening ability is maintained.

3.2 Microstructure

The surface deformation of the AZ31 magnesium alloy sheet differed from the deformation observed at the center during HPR. The microstructural evolution of the AZ31 magnesium alloy sheet along the ND was a key factor influencing the mechanical properties. Figures 3(a−d) illustrate the inverse pole figure (IPF) and grain size distribution of 50%-sheets. The sheet was predominantly made up of FG near its surface. Angles between 2° and 15° were categorized as low-angle grain boundaries (LAGBs, gray lines), while angles greater than 15° were categorized as high-angle grain boundaries (HAGBs, black lines). Figure 3 shows that HAGBs were more concentrated in the FG region. In the central region of the sheet, the grain size notably increased, and the volume fraction of HAGBs decreased significantly, which is defined as the CG region. Figures 3(e, f) show the kernel average misorientation (KAM) of 50%-sheets, which indicates the distribution of geometrically necessary dislocations (GNDs) [35]. Figure 3 shows that the GNDs primarily accumulate in the large grains and are predominantly found at the boundary between the CG and FG regions.

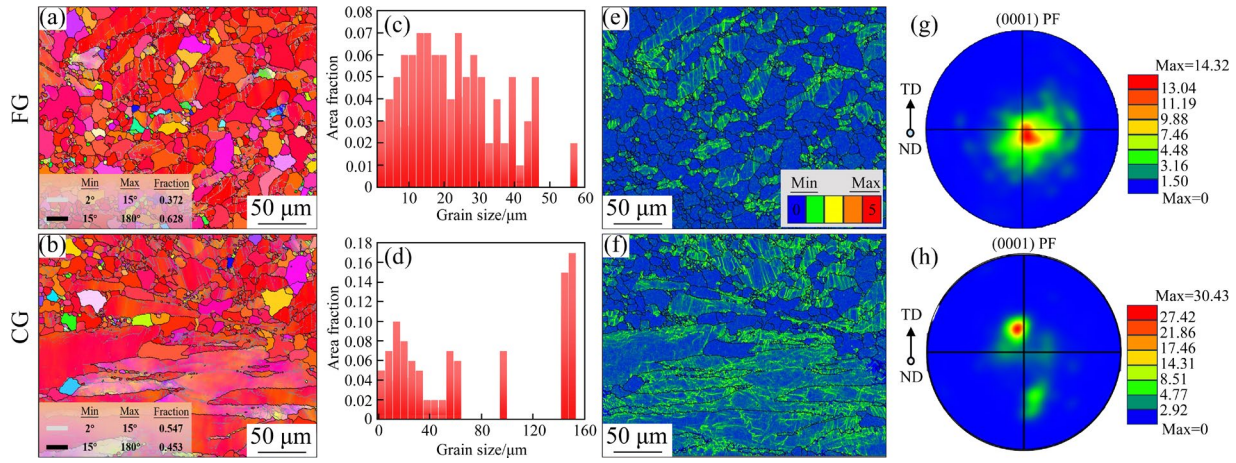

Fig. 3 Microstructures of 50%-loaded sheets in FG (a, c, e, g) and CG (b, d, f, h) regions: (a, b) IPF map; (c, d) Statistical map of grain size; (e, f) KAM map; (g, h) (0001) pole diagram

Previous studies have revealed the reason for the excellent strength and ductility coordination of gradient structure magnesium alloys with HPR; that is, the plastic incompatibility between the FG and CG regions induces GNDs to accumulate at the boundary of the FG/CG, resulting in back stress that improves the strength of the AZ31 magnesium alloy, and the resulting back stress hardening effectively avoids necking during the stretching process, which helps to improve ductility.

Figures 3(g, h) show the (0001) pole diagram of different regions of 50%-sheets. There were differences in texture types between the FG and CG regions. In the FG region, basal textures were mainly present. In contrast, in the CG region, many grains deviate from the basal orientation along the ND, which shows bimodal texture characteristics. The maximum texture intensity in the FG region was 14.32 m.r.d. (multiple random densities), whereas that in the CG region was 30.43 m.r.d. The difference in texture type and strength along the ND was an essential factor affecting the mechanical properties of the AZ31 magnesium alloy. The variation in the texture distribution along the ND and the change mechanism need to be analyzed further.

3.3 Texture distribution

The orientation distribution function (ODF) provides direct visualization of texture types and distributions. Figure 4 shows the texture types of the AZ31 magnesium alloy samples rolled by HPR to different extents. Figures 4(a, b) show the ODF figures for the FG region and CG region of the samples. The two most critical angles of the HCP structure, Φ=0° and Φ= 30°, were selected on the $\varphi 2$ section of the ODF. The standard texture type characteristics of HCP metals at these angles are presented in Fig. 4(c).

As depicted in Fig. 4(a), the main texture composition of the FG region in the 40%-sheets consisted of the $\{0001\}\langle 11\bar{2}0\rangle$ basal texture and the $\{10\bar{1}0\}\langle 11\bar{2}0\rangle$ prismatic texture. In the 50%-sheets, the texture transitioned from the $\{0001\}\langle 11\bar{2}0\rangle$ basal and $\{10\bar{1}0\}\langle 11\bar{2}0\rangle$ prismatic textures to a broader range, including the $\{10\bar{1}1\}\langle 11\bar{2}0\rangle$ pyramidal texture. This increase in texture variety creates favorable conditions for the activation of the pyramidal slip system. As the reduction continued, the texture in the 60%-sheets became simpler, primarily characterized by the $\{10\bar{1}0\}\langle 11\bar{2}0\rangle$ prismatic texture.

As shown in Fig. 4(b), in the CG region, the texture types under the three conditions were relatively singular, the distribution was relatively concentrated, the primary values were $\{0001\}\langle 11\bar{2}0\rangle$ texture, $\{10\bar{1}0\}\langle 11\bar{2}0\rangle$ texture, and no $\{10\bar{1}0\}\langle 11\bar{2}0\rangle$ texture appeared. From the perspective of texture strength, the texture strength of the samples first decreases but then increases with decreasing reduction. The texture strength of the 50%-sheets was the smallest, with a texture strength of 4.88 m.r.d. in the FG region and 12.61 m.r.d. in the CG region. This result indicates that the non-uniform deformation of each part of the plate affects the texture type and distribution.

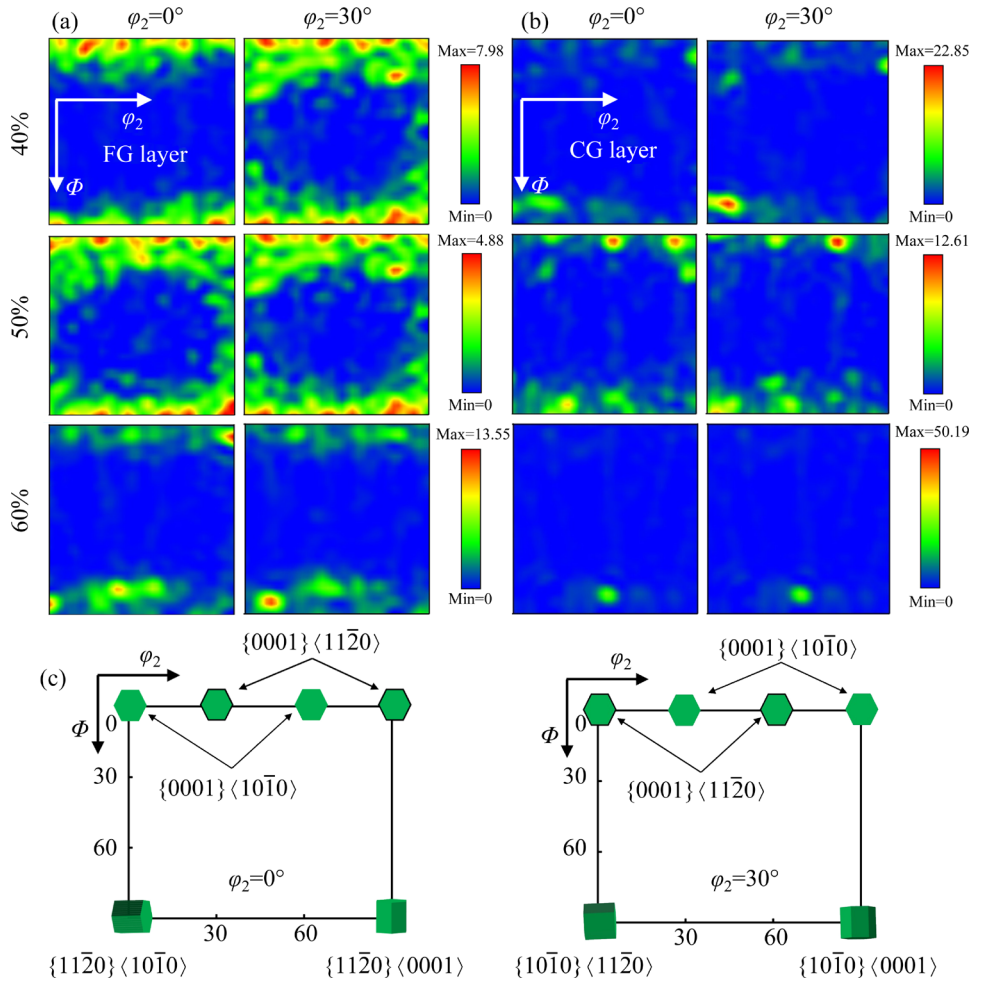

Fig. 4 ODF in different regions of AZ31 magnesium alloy sheets rolled by HPR: (a) ODF distribution in FG region; (b) ODF distribution in CG region; (c) Texture type

4 Discussion

4.1 Influence of recrystallization behavior on texture

Previous research has shown that an increase in rolling reduction provides a great recrystallization driving force, thus changing the orientation of recrystallized grains and affecting texture evolution [36]. Understanding the recrystallization behavior of gradient microstructure sheets and effectively controlling texture changes are highly important. Figures 5(a, b) show the recrystallization structure in the FG and CG regions of the 50%-sheets, and Figs. 5(c, d) show the corresponding column charts of the recrystallization volume fraction.

The recrystallized grains in the FG region were densely distributed, with a volume fraction reaching 64.7%. In contrast, the recrystallization proportion in the CG region decreased significantly, accompanied by a reduction in the number of substructures and deformed structures. Based on the findings in Section 3.2, it is concluded that variations in recrystallization volume fraction play a crucial role in determining the texture type and strength. The sample was divided into a recrystallization region and a non-recrystallization region according to the grain orientation spread (GOS), as shown in Figs. 5(e−h). GOS <1° was considered to recrystallized grains, and the remaining grains were considered substructures and deformed structures that had completed recovery or deformation. As shown in Fig. 5(e), the recrystallization region was mainly composed of FG with a texture strength of 14.52 m.r.d. The texture strength in the CG recrystallization region was notably lower (19.05 m.r.d.) than that in the non-recrystallization region (Figs. 5(g, h)). This difference indicates that

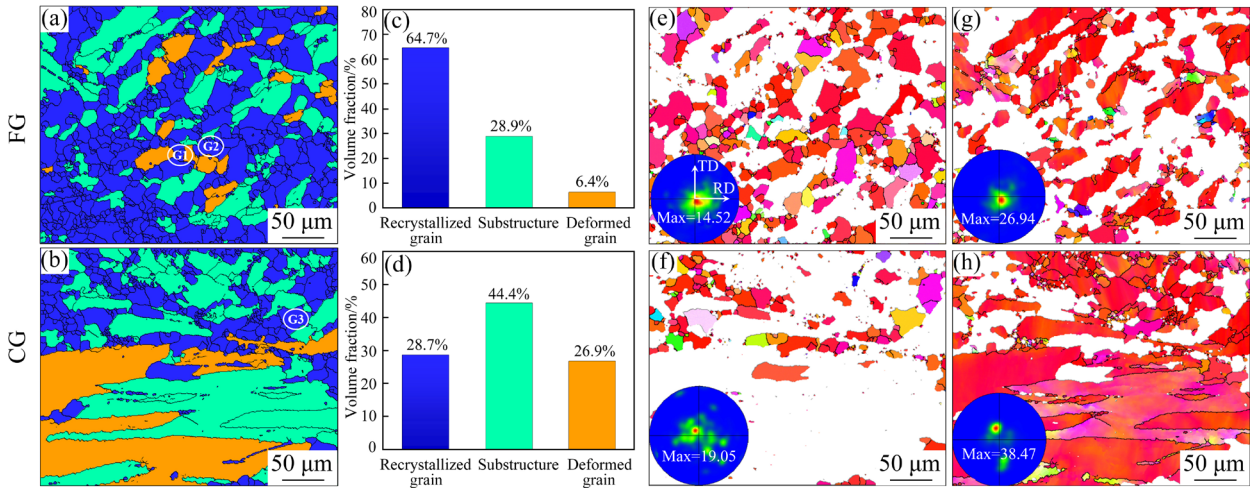

Fig. 5 Effect of recrystallization behavior on texture type in FG (a, c, e, g) and CG (b, d, f, h) regions: (a, b) Recrystallization distribution; (c, d) Proportion of recrystallization; (e, f) IPF of recrystallization region; (g, h) IPF of non-recrystallization region

the recrystallization process has a beneficial effect on basal texture weakening. Analysis of the polar diagram distributions indicates that grains in the non-recrystallization region exhibited more concentrated orientations, with an overall deflection toward RD. Conversely, the polar diagram distribution in the recrystallization region displayed a diffuse pattern, indicating a random orientation of the recrystallized grains.

As illustrated in Fig. 5, three representative regions were chosen to analyze the variations in grain orientation and texture type. Figure 6 displays the inverse pole figure (IPF), kernel average misorientation (KAM), and (0001) scatter diagrams of the corresponding grains. Figures 6(a, b) are selected from the recrystallization region of the fine-grain (FG) region, while Fig. 6(c) corresponds to the recrystallization region of the CG region. The (0001) scatter plot for Fig. 6(a) shows that the orientation distribution of the newly recrystallized grains was closely aligned with that of the adjacent parent grains. As seen in Fig. 6(d), Grains 3 and 4 represent examples of small recrystallized grains. Specifically, when the G2 parent grain has a basal plane orientation, the newly formed recrystallized grains align similarly with the parent grain orientation. This is in line with the continuous dynamic recrystallization mechanism. A sufficient driving force for recrystallization allows sub-grain boundaries to absorb dislocations and form high-angle grain boundaries, which split the parent grains, leading to the formation of new recrystallized grains.

Figure 6(g) shows that recrystallized grains initiate at the grain boundaries of the G3 parent grain and gradually grow into deformed grains characterized by high strain. This discontinuous nucleation mechanism of recrystallization is typically observed in low-strain regions. The corresponding (0001) scatter plot reveals that the newly formed recrystallized grains display orientations that differ significantly from those of their parent grains, with a more scattered distribution on the pole plot. During this process, variations in the *c*-axis deflection angle of grains are the primary factors contributing to changes in texture type and strength.

4.2 Influence of grain deflection on texture component

During the rolling process, the *c*-axis of grains are deflected by the applied rolling forces, leading to alterations in the texture type and strength, which play a significant role in the formability of the sheets. Figure 7 illustrates the influence of grain deflection on the texture type and strength during the deformation of AZ31 magnesium alloy under different conditions via HPR. Figures 7(a) and (c) show the polar figures of the FG and CG regions of the sample. Regarding texture strength, the CG region showed a considerable increase in texture strength compared to the FG region under all conditions. The 50%-sheets, in particular, displayed lower texture strength than the other samples, with 14.32 and 30.43 m.r.d. in the FG and CG regions,

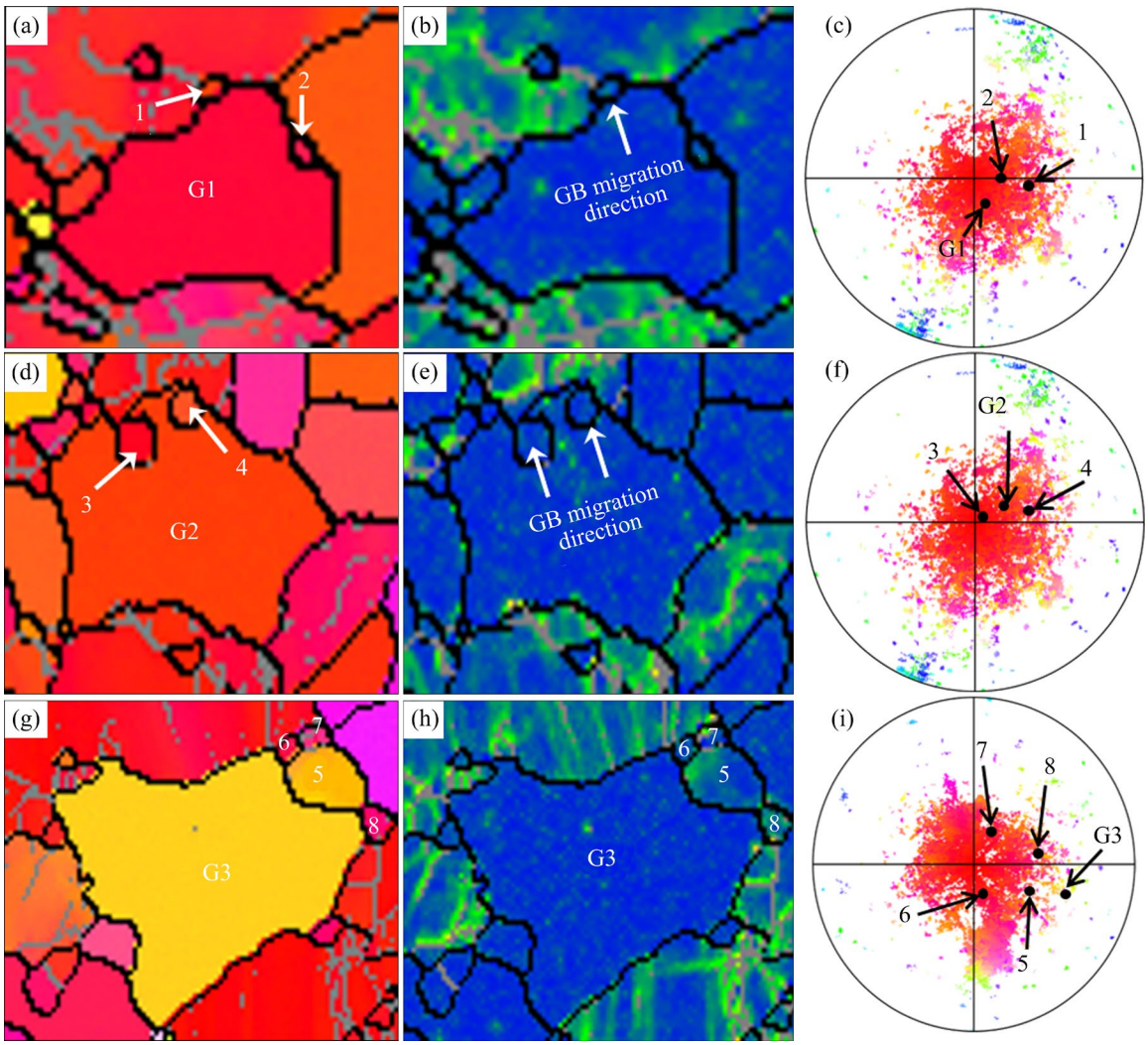

Fig. 6 IPF diagram (a, d, g), KAM diagram (b, e, h) and (0001) scatter diagram (c, f, i) of selected typical small regions in 50%-sheets: (a−f) G1 and G2 grain sets selected from recrystallization region of FG layer; (g−i) G3 grain sets selected from recrystallization region of CG layer

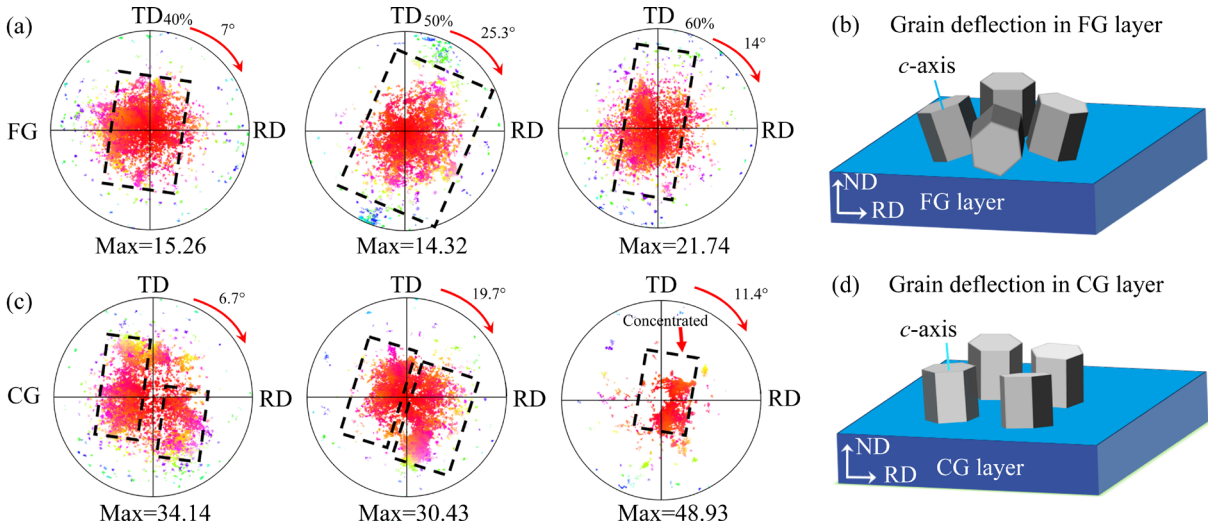

Fig. 7 Relationship between grain deflection and texture: (a) FG region; (b) Schematic of grain deflection in FG region; (c) CG region; (d) Schematic of grain deflection in CG region

respectively. The polar distributions of the FG and CG regions also varied. The FG region exhibited a basal texture with more scattered grain orientations, while the CG region displayed a bimodal structure (Fig. 7(c)) with more focused grain orientations. These variations in polar distribution suggest that grain rotation occurred during deformation.

The *c*-axis deflection angle of the grains in both the FG and CG regions initially increased, and then decreased. In the 50%-sheets, the *c*-axes of the grains were deflected from the ND to the RD by ~25.3° and ~19.7°, respectively, which was significantly larger than the deflection observed in the 40%-sheets. In the 60%-sheets, the *c*-axis deflection angle decreased, and texture strength increased. The polar figure in Figs. 7(a) and (c) shows that in the FG region of the 60%-sheets, the grain orientation was more concentrated, and the distribution on the polar diagram became more diffuse. In the CG region, grains with similar orientations were concentrated near the base, and no bimodal texture developed. As the reduction continued, most grains aligned to the same orientation, making it more difficult for the *c*-axis of the grains to deflect, leading to an increase in texture strength.

To gain further insight into the texture type and distribution in the AZ31 gradient structure of magnesium alloy sheets, the grains in both the FG and CG regions were classified into three groups based on the deflection angles of the *c*-axis and the (0001) basal plane. Angles between 0° and 30° were classified as texture component A (TCA), between 30° and 60° as texture component B (TCB), and between 60° and 90° as texture component C (TCC). The different texture components of the 50%-sheets are shown in Fig. 8. Figures 8(a−c) illustrate the

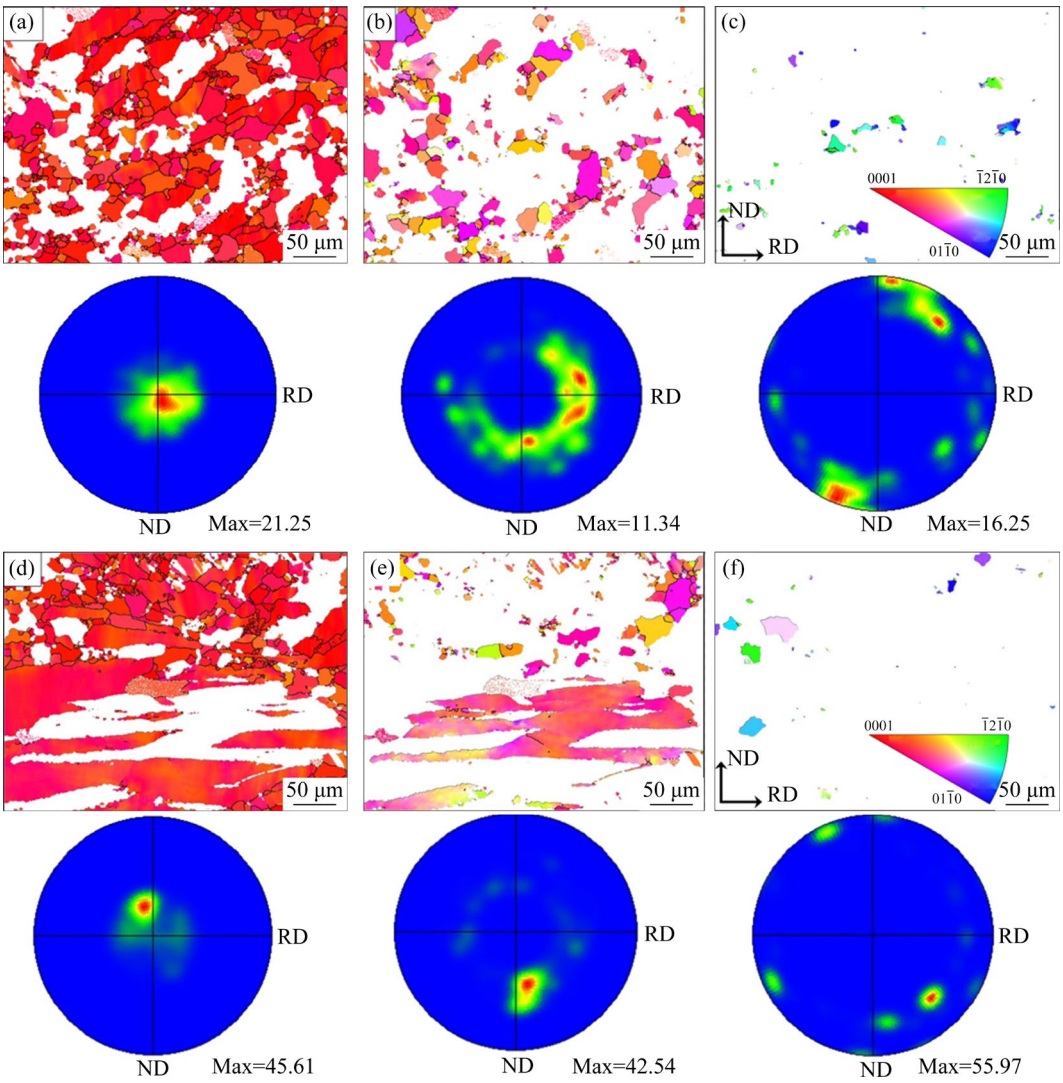

Fig. 8 IPF and (0001) polar figures showing relationship between grain orientation and texture: (a) FG, TCA; (b) FG, TCB; (c) FG, TCC; (d) CG, TCA; (e) CG, TCB; (f) CG, TCC

various texture components in the FG region. In this region, TCA was made up of larger grains, with a concentrated grain distribution and a maximum texture strength of 21.25 m.r.d. TCB was primarily composed of recrystallized grains, and its texture strength decreased to 11.34 m.r.d. Although the TCC component contained fewer grains, the pole figure (0001) in Fig. 8(c) shows a significant change in the texture type of TCC.

Figures 8(d−f) display the texture components in the CG region of the 50%-sheets, which show significant differences in texture strength and polar distribution compared to the FG region. The polar figure in Fig. 8(d) reveals a concentrated grain orientation with a texture strength of 45.61 m.r.d., which is considerably higher than the TCA in the FG region. Similarly, the pole figure in Fig. 8(e) shows a concentrated orientation for TCB, accompanied by a noticeable increase in texture strength. This suggests that, in the CG region, the limited extent of recrystallization results in smaller deflection angles for both the *c*-axis and the (0001) basal plane, leading to higher texture strength. A comparison with the results in Fig. 7 further highlights that grain size evolution plays a significant role in influencing texture type and strength.

4.3 Schmid factor

Due to the high critical shear stress (CRSS), the activation of prismatic and pyramidal slip systems in magnesium alloys is limited at room temperature, with the Schmid factor (SF) associated with texture having a notable influence on the activation of each slip system [37]. Figure 9 shows the SF calculations for the $\{0001\}\langle 11\bar{2}0\rangle$ basal slip, the $\{10\bar{1}0\}\langle 11\bar{2}0\rangle$ prismatic slip, and the $\{11\bar{2}2\}\langle 11\bar{2}3\rangle$ pyramidal slip systems in the FG and CG regions under various reductions in AZ31 magnesium alloy processed by HPR. Figures 9(a−c) indicate that the average SF for basal slip was the lowest in the 40%-sheets. As the reduction increased, there was little change in the average SF, with the highest average SF for basal slip

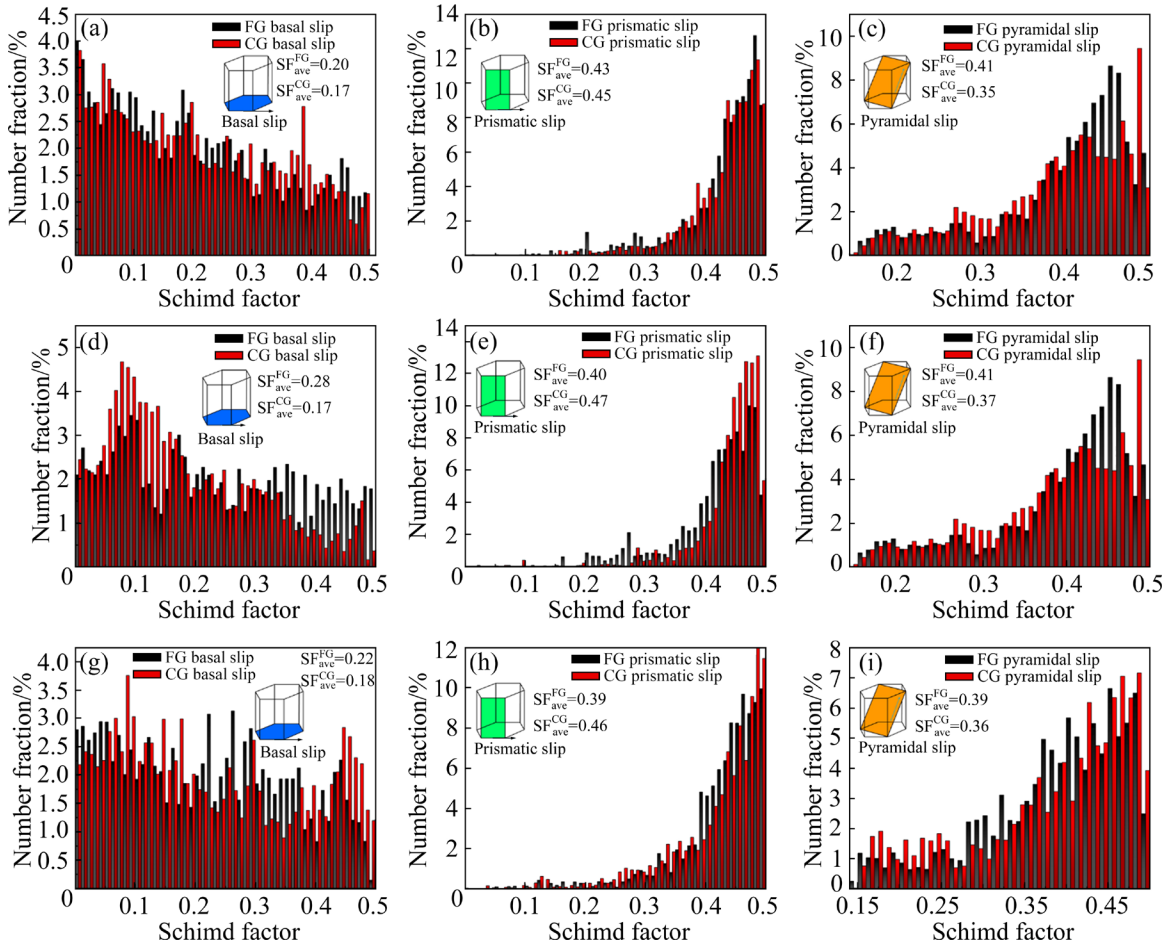

Fig. 9 Schmid factor of AZ31 magnesium alloy plate under different conditions: (a−c) 40%-sheets; (d−f) 50%-sheets; (g−i) 60%-sheets

observed in the 50%-sheets. Figures 9(d−f) demonstrate that prismatic slip maintained a consistently high average SF, peaking at 40%-sheets, where the SF reached 0.40 in the FG region and 0.47 in the CG region. This suggests that prismatic slip dominates the deformation process. In Figs. 9(g−i), the average SF for pyramidal slip in the CG region under different reductions was 0.35, 0.37, and 0.36, respectively, which were lower than those in the FG region (0.41, 0.41, and 0.39, respectively). This indicates that pyramidal slip is more easily activated in the FG region, a finding supported by the data in Fig. 4.

As shown in Fig. 9, increasing the reduction from 40% to 50% results in an increase in the SF for each slip system in the sample, accompanied by simultaneous activation of prismatic and pyramidal slip with high average SF values. However, in the 60%-sheets, the average SF of the pyramidal slip in the CG region decreased significantly because of the increased texture strength in the CG region, which hindered pyramidal slip activation. The FG region exhibits a higher average SF for both prismatic and pyramidal slip. The recrystallized grains in the FG region absorb non-basal dislocations, resulting in random grain orientation and promoting the activation of prismatic and pyramidal slip. As a result, the texture type and strength are modified.

4.4 Mechanistic analysis

The grain size and orientation influence the texture type and strength of the AZ31 magnesium alloy gradient structure produced by HPR, which subsequently affects its mechanical properties. Figure 10 displays the typical microstructure at the FG/CG interface and the corresponding KAM map for the 50%-sheets. The FG/CG interface creates a notable strain gradient along the ND of the sample, and GNDs from the same dislocation source accumulate at the interface to adapt to this strain gradient [38]. The back stress produced in AZ31 magnesium alloy, with its long-range and organized arrangement, enhances the mechanical properties. The grain distribution and dislocation evolution at the interface are depicted in Fig. 10(c).

Figure 10(d) shows the grain orientation of the magnesium alloy via HPR. The grain size of the FG region was small, the driving force of recrystallization was sufficient under the influence of the hard plate, the proportion of recrystallization grains was high, and the grain orientation was random. A random texture enhances the activity of basal sliding and facilitates its interaction with non-basal plane sliding, thereby making the activation of

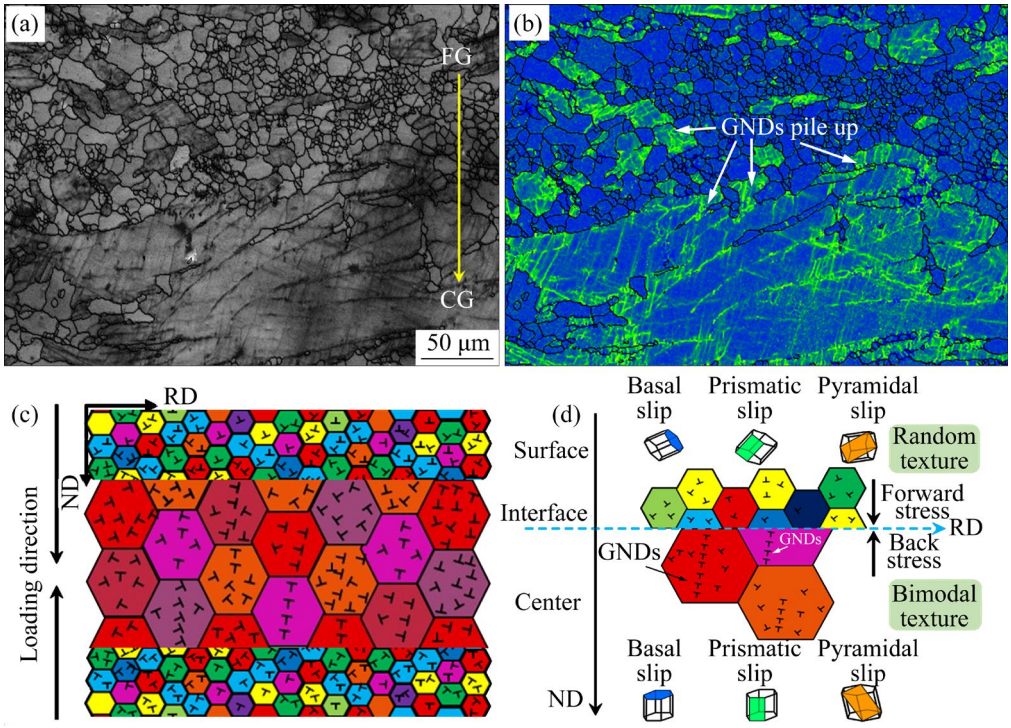

Fig. 10 Interface characteristics and texture evolution of 50%-sheets: (a) FG/CG interface microstructure; (b) KAM diagram; (c) Schematic diagram of mechanism distribution and dislocation evolution; (d) Grain orientation diagram

non-basal sliding easier. In the CG region, due to the effects of grain size and the limited driving force for recrystallization, the grain orientation was more concentrated, predominantly exhibiting prismatic and basal slip, resulting in the formation of a more concentrated texture in the CG region. The distribution of different texture types in the FG and CG regions results in a more significant difference at the interface, which affects the activation of different slip modes and helps to improve the mechanical properties of magnesium alloy sheets with gradient structures.

5 Conclusions

(1) The tensile strength and elongation of the AZ31 magnesium alloy with 673 K rolling temperature and 50% reduction were measured as 268.3 MPa and 28.3%, respectively. The microstructure displayed a gradient distribution in grain size and texture composition along the ND. The texture strength was recorded at 14.32 m.r.d. for the FG region and 30.43 m.r.d. for the CG region.

(2) The addition of a hard plate induced varying deformations along the ND in the magnesium alloy sheets, refining recrystallized grains in the FG region and significantly weakening the texture. The driving force for recrystallization was inadequate in the CG region. Simultaneously, the rolling force caused deflection of the *c*-axis in the grains, with a significant deflection angle observed in the FG region and a reduced angle in the CG region, which contributed to a noticeable increase in texture strength.

(3) As the reduction increased, the average Schmid factor of the $\{10\bar{1}0\}\langle 11\bar{2}0\rangle$ prismatic slip system rose in both the FG and CG regions. The basal texture plane inclined, resulting in the predominance of $\{10\bar{1}0\}$ prismatic textures. Additionally, the $\{11\bar{2}2\}\langle 11\bar{2}3\rangle$ pyramidal slip system in the FG region was activated. At a 60% reduction, the SF of the FG pyramidal slip system declined to 0.37, leading to increased complexity in the activation of the pyramidal slip system.

(4) Variations in grain size distribution between the FG and CG regions modified grain orientation, producing distinct texture components in different areas of the gradient structure of the magnesium alloy sheet. The interplay of multiple texture components altered the slip mode, amplifying the gradient strain distribution at the FG/CG interface and facilitating the accumulation of GNDs. This phenomenon positively influenced the properties of gradient magnesium alloy sheets.

CRediT authorship contribution statement

Wen-tao NIU: Methodology, Investigation, Data curation, Formal analysis, Writing – Original draft; **Feng LI:** Supervision, Funding acquisition; **Jia-yang ZHANG:** Writing – Review & editing; **Lu SUN:** Investigation, Formal analysis; **Zi-yi WANG:** Validation, Software.

Declaration of competing interest

The authors declare that they have no known competing financial interests or personal relationships that could have appeared to influence the work reported in this paper.

Acknowledgments

This work was supported by the Natural Science Foundation of Heilongjiang Province, China (No. JQ2022E004)

References

[1] WANG Jia-hao, WU Rui-zhi, FENG Jing, ZHANG Jing-huai, HOU Le-gan, LIU Mei-duo. Recent advances of electromagnetic interference shielding Mg matrix materials and their processings: A review [J]. Transactions of Nonferrous Metals Society of China, 2022, 32(5): 1385−1404.

[2] HUANG Lan-ping, HE Long-long, LI Song, LIU Wei-sheng, HUANG Jing, CHEN Song-yi. Effects of pre-stretch on microstructure, mechanical properties and corrosion resistance of 2A14 aluminum alloy [J]. Transactions of Nonferrous Metals Society of China, 2024, 34(4): 1065−1080.

[3] WEI Liang-yu, GAO Zi-yuan. Recent research advances on corrosion mechanism and protection, and novel coating materials of magnesium alloys: A review [J]. RSC Advances, 2023, 13: 8427−8463.

[4] ATRENS A, SHI Zhi-ming, MEHREEN S, JOHNSTON S, SONG Guang-ling, CHEN Xian-hua, PAN Fu-sheng. Review of Mg alloy corrosion rates [J]. Journal of Magnesium and Alloys, 2020, 8: 989−998.

[5] SONG Jiang-feng, SHE Jia, CHEN Dao-lun, PAN Fu-sheng. Latest research advances on magnesium and magnesium alloys worldwide [J]. Journal of Magnesium and Alloys, 2020, 8: 1−41.

[6] NIE jian-feng, SHIN K S, ZENG Zhuo-ran. Microstructure, deformation, and property of wrought magnesium alloys [J]. Metallurgical and Materials Transactions A, 2020, 51: 6045−6109.

[7] JIA Chen, XIONG Zhi-ping, YANG De-zhen, WANG Yang-wei, CHENG Xing-wang. Effect of rolling temperature and reduction on brick-and-mortar Ti2Ni/TiNi composite[J].

Transactions of Nonferrous Metals Society of China, 2023, 33(7): 2064−2075.

[8] BAMBERGER M, DEHM G. Trends in the development of new Mg alloys [J]. Annual Review of Materials Research, 2008, 38: 505−533.

[9] CHAI Ya-qin, BOEHLERT C J, WAN Yi-fu, HUANG G H, ZHOU Hao, ZHENG Jiang, WANG Qu-dong, YIN Dong-di. Anomalous tension twinning activity in extruded Mg sheet during hard-orientation loading at room temperature[J]. Metallurgical and Materials Transactions A, 2021, 52: 449−456.

[10] CHANG T C, WANG J Y, O C M, LEE S. Grain refining of magnesium alloy AZ31 by rolling[J]. Journal of Materials Processing Technology, 2003, 140(1/2/3): 588−591.

[11] DEL VALLE J A, PÉREZ-PRADO M T, RUANO O A. Accumulative roll bonding of a Mg-based AZ61 alloy[J]. Materials Science and Engineering: A, 2005, 410: 353−357.

[12] ZHANG Yu-bo, NI Ran, ZHENG Xi-hao, HUA Shen, ZHOU Hao, ZENG Ying, YIN Dong-di. Understanding the reversed tension–compression asymmetry of an extruded Mg−10Y sheet from the perspective of slip activity and plastic heterogeneity [J]. Metallurgical and Materials Transactions A, 2024, 55(5): 1673−1689.

[13] YANG Wu, QUAN Gao-feng, JI Bongg-yu, WAN Yi-fu, ZHOU Hao, ZHENG Jiang, YIN Dong-di. Effect of Y content and equal channel angular pressing on the microstructure, texture and mechanical property of extruded Mg−Y alloys[J]. Journal of Magnesium and Alloys, 2022, 10(1): 195−208.

[14] LIU Yan-xiao, LIU Yuan-ming, WANG Zhen-hua, LIU Yan-ping, WANG Tao, HUANG Qing-xue. Stress analysis and microstructure evolution of Cu/Al composite plate during corrugated rolling [J]. Transactions of Nonferrous Metals Society of China, 2023, 33(5): 1460−1471.

[15] SINGH A K, SCHWARZER R A. Schwarzer. Evolution of texture in pure magnesium during rolling [J]. International Journal of Materials Research, 2005, 96(4): 345−351. (in German)

[16] LIANG Shu-jin, SUN Hong-fei, LIU Zu-yan, WANG Er-de. Mechanical properties and texture evolution during rolling process of an AZ31 Mg alloy [J]. Journal of Alloys and Compounds, 2009, 472(1/2): 127−132.

[17] ZHANG Yun, JIANG Hai-tao, KANG Qiang, WANG Yu-jiao, YANG Yong-Gang, TIAN Shi-wei. Microstructure evolution and mechanical property of Mg−3Al alloys with addition of Ca and Gd during rolling and annealing process [J]. Journal of Magnesium and Alloys, 2020, 8(3): 769−779.

[18] HOU Jin-xiong, QIAO Jun-wei, LIAN Jun-he, LIAW P K. Revealing the relationship between microstructures, textures, and mechanical behaviors of cold-rolled $Al_{0.1}$CoCrFeNi high-entropy alloys [J]. Materials Science and Engineering: A, 2021, 804: 140752.

[19] LIU Di, LIU Zu-yan, WANG Er-de. Effect of rolling reduction on microstructure, texture, mechanical properties and mechanical anisotropy of AZ31 magnesium alloys [J]. Materials Science and Engineering: A, 2014, 612: 208−213.

[20] ZHANG An-xin, LI Feng, HUO Peng-da, NIU Wen-tao, GAO Rong-he. Response mechanism of matrix microstructure evolution and mechanical behavior to Mg/Al composite plate by hard-plate accumulative roll bonding [J]. Journal of Materials Research and Technology, 2023, 23: 3312−3321.

[21] NIU Wen-tao, LI Feng, LI Yuan-qi, WANG Zi-yi, SUN Lu. Grain boundary-mediated strain response mechanism of AZ31 gradient- structure Mg alloy plate under uniaxial tensile loading [J]. Journal of Magnesium and Alloys, 2025, 13: 2283−2294

[22] FU Wei, DANG Peng-fei, GUO Sheng-wu, REN Zi-jun, FANG Da-qing, DING Xiang-dong, SUN Jun. Heterogeneous fiberous structured Mg−Zn−Zr alloy with superior strength-ductility synergy [J]. Journal of Materials Science & Technology, 2023, 134: 67−80.

[23] SUN Lu, LI Feng, ZHANG An-xin, ZHANG Jia-yang, WANG Zi-yi. Synergistic mechanism of strengthening and toughening of tissue regulation response to Mg/Al composite laminates by hard plate accumulative roll bonding [J]. Materials Science and Engineering A, 2024, 892: 146105.

[24] ZHAO Dong-sheng, YAN Jiu-chun, LIU Yu-jun, JI Zhou-shang. Interfacial structure and mechanical properties of hot-roll bonded joints between titanium alloy and stainless-steel using niobium interlayer [J]. Transactions of Nonferrous Metals Society of China, 2014, 24(9): 2839−2844.

[25] YIN Dong-di, BOEHLERT Carl-J, LONG Lian-jie, HUANG G H, ZHOU Hao, ZHENG Jiang, WANG Qu-dong. Tension-compression asymmetry and the underlying slip/twinning activity in extruded Mg−Y sheets [J]. International Journal of Plasticity, 2021, 136: 102878.

[26] LIU Shuai-shuai, XIA Da-biao, YANG Hong, HUANG Guang sheng, YANG Fei-xiang, CHEN Xian-hua, TANG Ai-tao, JIANG Bin, PAN Fu-sheng. Mechanical properties and deformation mechanism in Mg−Gd alloy laminate with dual-heterostructure grain size and texture [J]. International Journal of Plasticity, 2022, 157: 103371.

[27] DUAN Meng, LUO Lan, LIU Yong. Microstructural evolution of AZ31 Mg alloy with surface mechanical attrition treatment: Grain and texture gradient [J]. Journal of Alloys and Compounds, 2020, 823: 153691.

[28] AMIRI M M, FERESHTEH-SANIEE F. Influence of roll speed difference on microstructure, texture and mechanical properties of 7075 aluminum plates produced via combined continuous casting and rolling process [J]. Transactions of Nonferrous Metals Society of China, 2021, 31(4): 901−912.

[29] RONG Jian, WANG Peng-yue, ZHA Min, WANG Cheng, XU Xin-yu, WANG Hui-yuan, JIANG Qi-chuan. Development of a novel strength ductile Mg−7Al−5Zn alloy with high superplasticity processed by hard-plate rolling (HPR) [J]. Journal of Alloys and Compounds, 2018, 738: 246−254.

[30] WANG Hui-yuan, YU Zhao-peng, ZHANG Lei, LIU Chun-guo, ZHA Min, WANG Cheng, JIANG Qi-chuan. Achieving high strength and high ductility in magnesium alloy using hard-plate rolling (HPR) process [J]. Scientific Reports, 2015, 5(1): 17100.

[31] LI Yong-kang, ZHA Min, RONG Jian, JIA Hai-long, JIN Zhong-zheng, ZHANG Hong-min, MA Pin-kui, XU Hong, FENG Ting-ting, WANG Hui-yuan. Effect of large thickness-reduction on microstructure evolution and tensile properties of Mg−9Al−1Zn alloy processed by hard-plate rolling [J]. Journal of Materials Science & Technology, 2021, 88: 215−225.

[32] WANG Tong, ZHA Min, GAO Yi-Peng, WANG Si-qing, JIA

Hai-long, WANG Cheng, WANG Hui-yuan. Deformation mechanisms in a novel multiscale hetero-structured Mg alloy with high strength-ductility synergy [J]. International Journal of Plasticity, 2023, 170: 103766.

[33] HUO Peng-da, LI Feng, XU Hong-yu, NIU Wen-tao, GAO Rong-he. Achieving large-scale gradient structure in the AZ31 magnesium alloys for extraordinary strength-ductility synergy by hard plate rolling [J]. Journal of Alloys and Compounds, 2023, 944: 169176.

[34] ZHA Min, ZHANG Xuan-he, ZHANG Hang, YAO Jia, WANG Cheng, WANG Hui-yuan, FENG Ting-ting, JIANG Qi-chuan. Achieving bimodal microstructure and enhanced tensile properties of Mg−9Al−1Zn alloy by tailoring deformation temperature during hard plate rolling (HPR) [J]. Journal of Alloys and Compounds, 2018, 765: 1228−1236.

[35] MOLNÁR P, JÄGER A, LEJČEK P. The role of low-angle grain boundaries in multi-temperature equal channel angular pressing of Mg–3Al–1Zn alloy [J]. Journal of Materials Science, 2012, 47: 3265−3271.

[36] GUO Li-li, FUJITA F. Influence of rolling parameters on dynamically recrystallized microstructures in AZ31 magnesium alloy sheets [J]. Journal of Magnesium and Alloys, 2015, 3(2): 95−105. (Journal publication)

[37] HAN Jing, SUN Jia-peng, SONG Yuan-ming, XU Bo, YANG Zhen-quan, XU Song-song, HAN Ying, WU Guo-song, ZHAO Ji-yun. Achieving gradient heterogeneous structure in Mg alloy for excellent strength-ductility synergy [J]. Journal of Magnesium and Alloys, 2023, 11(7): 2392−2403.

[38] WU Xiao-lei，JIANG Ping, CHEN Liu, YUAN Fu-ping, ZHU Yun-tian. Extraordinary strain hardening by gradient structure [M]//Heterostructured Materials. New York: Jenny Stanford Publishing, 2021: 53−71.

梯度组织 AZ31 镁合金板材多重织构组分下的晶粒取向及滑移模式演变

牛文涛[1]，李 峰[1,2,3]，张佳阳[1]，孙 璐[1]，王梓懿[1]

1. 哈尔滨理工大学 材料科学与化学工程学院，哈尔滨 150040；
2. 哈尔滨理工大学 先进制造与智能技术教育部重点实验室，哈尔滨 150080；
3. 哈尔滨理工大学 黑龙江省轻金属材料改性与绿色成形技术重点实验室，哈尔滨 150040

摘 要：为了探究多重织构组分条件下晶粒取向及滑移模式的演变规律，通过衬板轧制(HPR)制备了梯度组织结构 AZ31 镁合金板材，研究不同压下量下板材织构及滑移模式的变化。结果表明，所得 AZ31 镁合金板材具有自外延梯度结构特征且在轧制温度 673 K 和压下量 50%时的力学性能最佳。在板材 ND 上织构类型及强度有显著变化，粗晶区呈现沿轧制方向的双峰织构。织构组分差异加剧细晶−粗晶界面处的应变分布，影响晶粒取向及不同滑移模式的激活，有助于改善梯度结构镁合金板材的力学性能，为高性能梯度组织镁合金板材成形制造提供了一种新思路。

关键词：衬板轧制；AZ31 镁合金板材；梯度结构；织构组分；晶粒取向

(Edited by Xiang-qun LI)